Available online at www.sciencedirect.com

ScienceDirect

Procedia Manufacturing 34 (2019) 647–654

Procedia MANUFACTURING

www.elsevier.com/locate/procedia

47th SME North American Manufacturing Research Conference, Penn State Behrend Erie, Pennsylvania, 2019

Layerless Additive Manufacturing of Metal Alloy Lattices Using Immiscible-Interface Assisted Direct Metal Drawing

Li He, Fan Fei, Wenbo Wang, Xuan Song*

Department of Industrial and Systems Engineering, University of Iowa, Iowa City, IA 52242, USA

Center for Computer Aided Design, University of Iowa, Iowa City, IA 52242, USA

* Corresponding author. Tel.: +319-335-5680; fax: +0-319-335-6086. *E-mail address:* xuan-song@uiowa.edu

Abstract

State-of-the-art metal alloy additive manufacturing (AM) techniques construct a three-dimensional structure through sintering or melting dry metal powders in a layer-by-layer fashion, which typically results in several AM-specific issues in the final structure, such as staircase effect, residual stress and highly-orientated microstructures. In this paper, we present a new extrusion-based metal AM process, named Immiscible-interface assisted Direct Metal Drawing (II-DMD), which fabricates metal alloy structures, in particular lattice structures, in a layerless manner. In the II-DMD process, metal lattice structures are fabricated by continuously extruding a metal colloidal suspension within a second immiscible matrix colloidal suspension. The shape of the metal colloidal suspension is stabilized due to the presence of an immiscible interface between the two colloidal suspension systems. Dense metal lattice structures can be achieved via post-consolidation of the self-stabilized metal-matrix systems, including liquid-phase drying and metal-phase sintering. The II-DMD process is presented and the immiscible-interface-assisted self-stabilization mechanism is studied. The post-consolidation processes are discussed. Several test cases were fabricated and characterized.

Keywords: immiscible interface; direct metal drawing; colloidal suspension; self-stabilization; sintering

1. Introduction

Conventional additive manufacturing (AM) processes of metal alloys[1] build a three-dimensional (3D) structure through selectively sintering or melting dry metal powders in a layer-by-layer manner using a high-energy beam. The layer-based fabrication manner and the localized high-temperature heating used in those processes result in several AM-specific issues in final structures, such as staircase effect, residual stress and highly-orientated columnar microstructures. The staircase effect reduces surface finish of final components and introduce stress concentration; residual stress and highly-orientated microstructures negatively influence mechanical properties of final objects [2, 3].

In this paper, we report a new AM process for fabricating metal alloy structures (in particular lattice structures) in a layerless fashion, i.e., immiscible-interface assisted direct metal drawing (II-DMD). This layerless metal AM process offers the potential to mitigate the inherent defects associated with layer-based fabrication approaches. In this new process, an alloy-powder-based suspension is first deposited continuously in 3D space within a secondary matrix suspension and then uniformly densified through heat treatment. By tailoring the two colloidal systems, a suitable immiscible interface can be established between the metal-powder suspension and the secondary matrix suspension, which consequently enables the self-stabilization of

10.1016/j.promfg.2019.06.106

the deposited 3D geometry. Similar fabrication techniques [4-12] have been used to create microvascular networks[12], soft sensors[10], robots[11], and other 3D structures, which are however still limited to polymer materials (e.g. hydrogel) and have not yet been attempted to build metal structures.

The paper is organized as follows. Section 2 describes starting materials used in the II-DMD process and introduces the fabrication process; section 3 discusses the process modeling and optimization; section 4 demonstrates several testcases and their properties; conclusions and future work are discussed in section 5.

2. Methods

2.1 Starting materials

In this research, bronze is used as a model material to study layerless AM of 3D metal alloy lattice components via the II-DMD process. Aluminum oxide or alumina is used as a secondary matrix material, which acts as a support medium to maintain 3D geometry of the body material (e.g., bronze powders) throughout heat treatment. Alumina is selected because of its high sintering temperature (> 1300ºC) in comparison to bronze powders. This temperature difference allows the secondary matrix material to remain loose after heat treatment and to be ultimately removed from target alloy components.

In the proposed II-DMD process, both bronze and alumina powders are prepared as a suspension. Silicon oil and water are employed as the dispersion medium of bronze-powder suspensions and alumina-matrix suspensions respectively to introduce an immiscible interface [13, 14] between bronze and alumina particles, which enables the self-stabilization of a deposited bronze-powder suspension in an alumina-matrix suspension. More details are discussed in section 2.3. Bronze-oil suspensions are prepared by mixing as-received bronze powders (BZ5890M, Chemical Store Inc. Clifton, NJ, USA) with silicone oil at a specific concentration in a magnetic stirrer for ~15 minutes. The composition and properties of the bronze powders are listed in Table 1. Alumina-water suspensions are prepared by mixing alumina powders (D50: 9µm, GE6, Baikowski, Charlotte, USA) with deionized water at a specific concentration in a magnetic stirrer for ~15 minutes.

Table 1. Composition and properties of used bronze powders

Chemical	Composition
Copper	90%
Tin	10%
Phosphorous	0.07%
Apparent density	5g/cc
Particle size	-325MESH

2.2 Fabrication process

A schematic illustration of the II-DMD process is shown in Fig. 1. A pressurized dispensing syringe (Ultimus I, Nordson Co., Westlake, Ohio, USA) is mounted on a three-degree-of-freedom (DoF) gantry system (E3, Nordson Co., Westlake, Ohio, USA). The syringe is loaded with a bronze-oil suspension and is controlled to continuously extrude the suspension along a given 3D tool path within an alumina-water suspension in a crucible, as depicted in Fig. 1a. The tool path of the syringe is created with a customized Matlab code. As the bronze-oil suspension is deposited, an immiscible water-oil interface is instantaneously established between the bronze and alumina particles, which locks the bronze and alumina particles in position and maintain the 3D shape of the deposited bronze-oil suspension, as shown in Fig. 1b. Rheological properties of both bronze and alumina suspensions are carefully tailored to avoid deformation of the deposited 3D shape during fabrication (e.g., fragments, bead up, diffusion, or sedimentation).

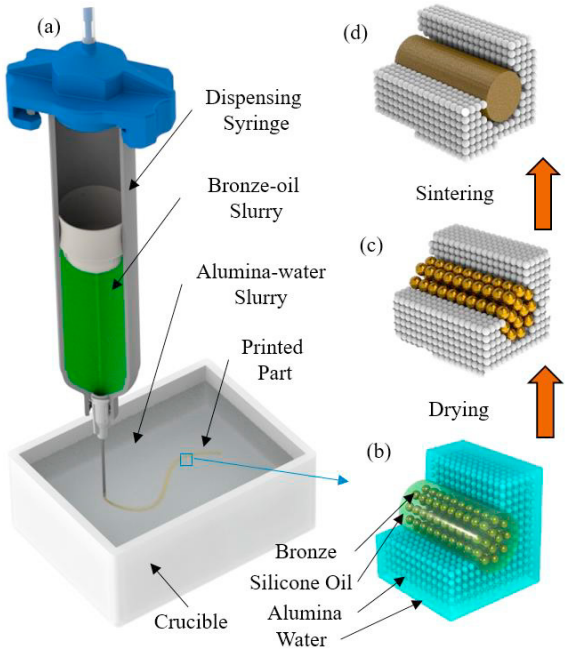

Fig. 1. Schematic illustration of the II-DMD process.

After the bronze-oil suspension is deposited, the crucible is heated in an oven to evaporate the liquid phases, including water in the alumina-water suspension and silicone oil in the bronze-oil suspension, leaving only dry bronze particles with a desired 3D shape embedded in a dry alumina powder bed, as depicted in Fig. 1c. Following that, a high-temperature sintering process is performed to densify the bronze particles with the surrounding alumina particles remaining loose (refer to Fig. 1d). The temperature schedules for both drying and sintering are presented in section 2.4. After removing the loose alumina particles, a dense bronze component can be obtained. Both the removed alumina powder and the leftover bronze suspension in the syringe can be

recycled and reused. Fig. 2 describes the flowchart for fabricating metal alloy components via the layerless II-DMD process.

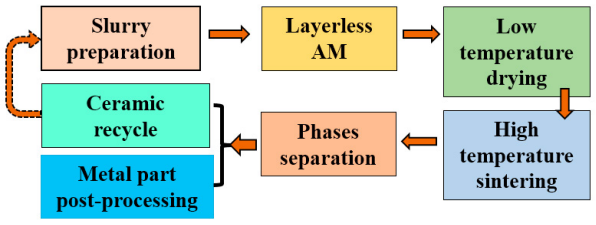

Fig. 2. A flowchart for the II-DMD fabrication process

Compared to conventional layer-based AM processes, the new II-DMD process has several potential advantages in building metal lattice structures, such as isotropic mechanical properties, low residual stress, no need of support structures and faster speed. As illustrated in Fig. 3, 3D metal alloy lattice components fabricated by layer-based AM processes show a surface staircase effect and usually exhibit anisotropic mechanical properties due to columnar microstructures caused by directional heat flow [15]. For complex lattices with overhanging features, sacrificial support structures are required to prevent distortion/curling resulting from thermal stresses [16]. All these drawbacks can be potentially overcome in the proposed II-DMD process through continuously extruding materials in 3D space instead of in a layer-by-layer manner.

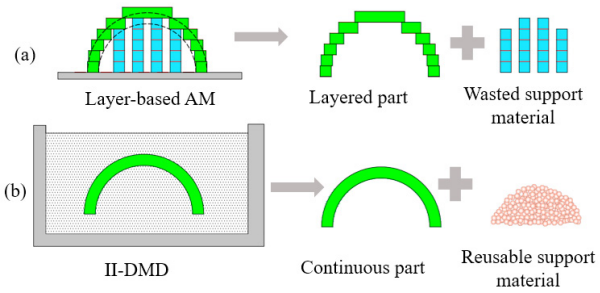

Fig. 3. A comparison between layer-based metal AM and II-DMD

2.3 Self-stabilization mechanism

To ensure the self-stabilization of an extruded bronze-powder suspension in an alumina-matrix suspension, different combinations of powder suspensions have been tested. Among all the tested suspensions, a metal-oil suspension dispensed in an alumina-water suspension achieves the best outcome. Oil and water forms an immiscible interface[13, 14] between the two suspensions, which acts as a barrier to separate bronze and alumina particles, as shown in Fig. 4.

The fundamental mechanism behind the immiscible-interface enabled self-stabilization of bronze-oil suspensions in alumina-water suspensions can be explained as follows. In the metal-oil suspension, the oil is pre-infused within highly-loaded metal particles, yielding a large surface tension Υ between bronze particles. This surface tension Υ and a buoyant force F_b from the liquid oil produce a resistance force F_{res} on each bronze particle that overcomes the gravitational force G and consequently locks relative distances between bronze particles. Meanwhile, due to the presence of this surface tension Υ between bronze particles and the immiscible oil-water interface, ceramic particles cannot break through the boundary and diffuse into the bronze phase without extra stirring. On the other hand, in the alumina-water suspension, alumina particles are uniformly distributed under a repulsive force F_{repl} resulting from particle surface charges. When the solid loading of alumina particles is sufficiently high, the repulsive force F_{repl} can reliably support an extruded structure of bronze-oil suspensions without distortion and deformation.

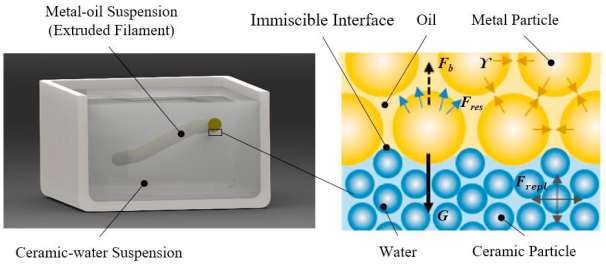

Fig. 4. Immiscible-interface assisted self-stabilization

2.4 Heat treatment

After a self-stabilized bronze-oil suspension with a desired 3D geometry is achieved, post processes of heat-treatment are conducted to obtain dense metal alloy components. The temperature schedules for the heat treatment are provided in Fig. 5.

The extruded bronze-oil suspension along with the alumina-water suspension are first heated in an oven to evaporate the liquid phases. The drying temperature schedule is given in Fig. 5a. Through this step, a dry bronze-powder compact with a desired 3D geometry is obtained, surrounded by a nearly dry alumina powder bed (refer to Fig. 1c). The alumina powder bed still contains a small amount of silicon oil that diffused from the bronze-oil suspension during drying.

After drying, both the bronze-powder compact and the alumina powder bed are heated together in an argon furnace. The heating temperature schedule is given in Fig. 5b. Since the used temperature (i.e., 950 ºC) is much lower than the sintering temperature of alumina powder (e.g., 1400 ºC), only bronze particles are sintered, with the alumina matrix powder remaining loose. During the high temperature sintering, the residual silicone oil in the alumina powder bed is completely decomposed. Finally, the alumina matrix powder is removed and recycled for future use, leaving the sintered bronze body as the final product.

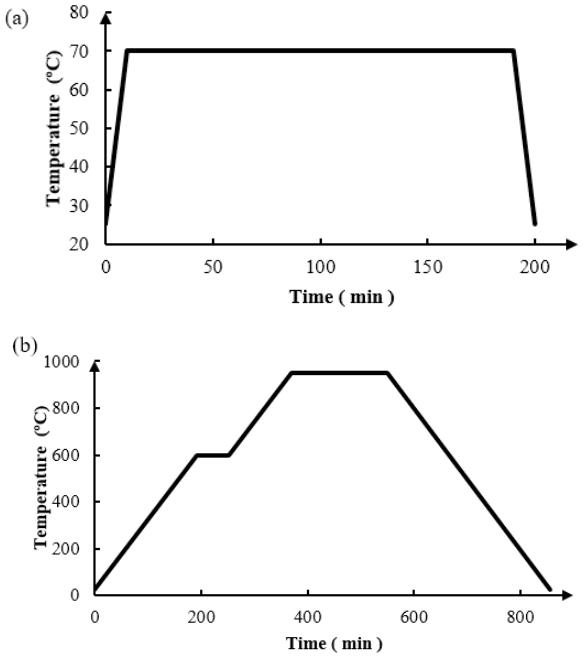

Fig. 5. (a) Temperature schedule for drying; (b) Temperature schedule for sintering.

3. Process Modeling

3.1 Material characterization

To enable a controllable extrusion through a pressurized dispenser, a bronze-oil suspension must possess a shear elastic modulus G' and yield stress τ that are approximately an order of magnitude larger than those of the secondary matrix suspension [6, 17] to ensure the bronze-oil suspension maintains its shape after it exits the nozzle. Meanwhile, an alumina-water suspension should exhibit a shear thinning behavior with a suitable yield stress, such that the bronze-powder suspensions can be supported after extrusion[18] and crevices generated by nozzle movement can be immediately healed. To identify material properties that enable a controllably stable extrusion, gravity settling and rheology behaviors of bronze-oil and alumina-water suspensions at different solid loadings (i.e., 90~95wt% bronze-oil suspensions and 30 ~ 45wt% alumina-water suspensions) were characterized. The characterization results are given in Fig. 6~8.

Gravity settling. Gravity settling behaviors of suspensions were determined by sedimentation tests. That is, suspensions at different solid loadings are thoroughly mixed and then allowed to stand undisturbed for 30 minutes. As can be seen in Fig. 6 and Fig. 7, bronze-oil suspensions with a solid loading less than 92wt% and alumina suspensions with a solid loading less than 30wt% tend to settle rapidly, while a solid loading higher than 95wt% for bronze suspensions and 45wt% for alumina suspensions yields a solid-like behavior. To avoid particle sedimentation and ensure the optimal stability and printability during the II-DMD process, a 94wt% bronze-oil suspension and a 40wt% alumina-water suspension are hence selected in this study.

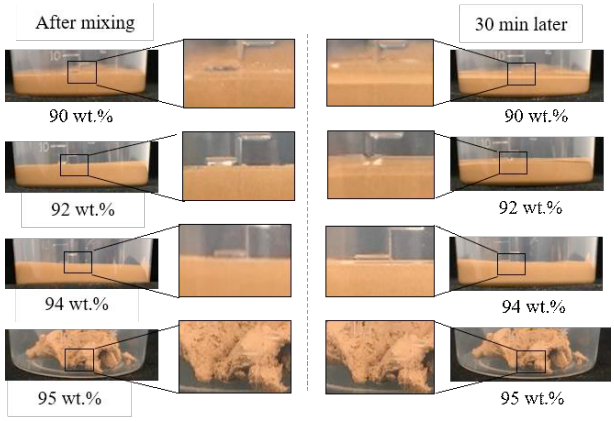

Fig. 6. Sedimentation tests of bronze oil suspensions.

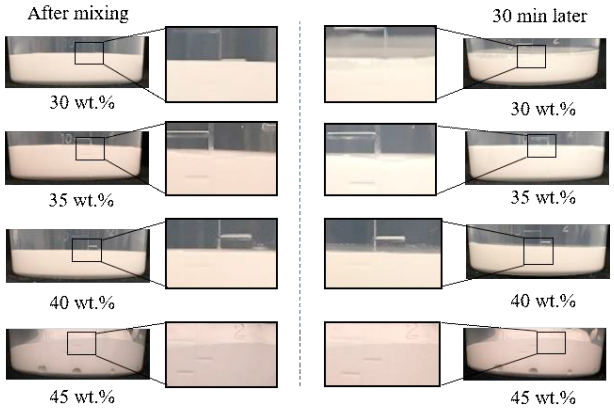

Fig. 7 Sedimentation tests of alumina-water suspensions.

Rheology properties. Rheology behaviors of a 40wt% alumina-water suspension and a 94wt% bronze-oil suspension were measured with a parallel-plate rheometer (MCR72, Anton Paar, Ashland, VA, USA) on a logarithmic scale. The shear rate was changed from 1 to 100 1/s. Fig. 8 suggests that the 40 wt.% alumina-water suspension and the 94% bronze-oil suspension exhibit a desired shear thinning behavior with a sufficiently high viscosity and yield stress suitable for the II-DMD process.

Suspensions with the selected solid loadings, i.e., 94wt% for bronze-oil suspensions and 40wt% for alumina-water suspensions, were used to study the process-structure relationships of the II-DMD process, including the effects of extrusion pressures p and printing nozzle speed v on extruded filament size y, and the effects of nozzle movement and liquid-phase drying on filament deformation.

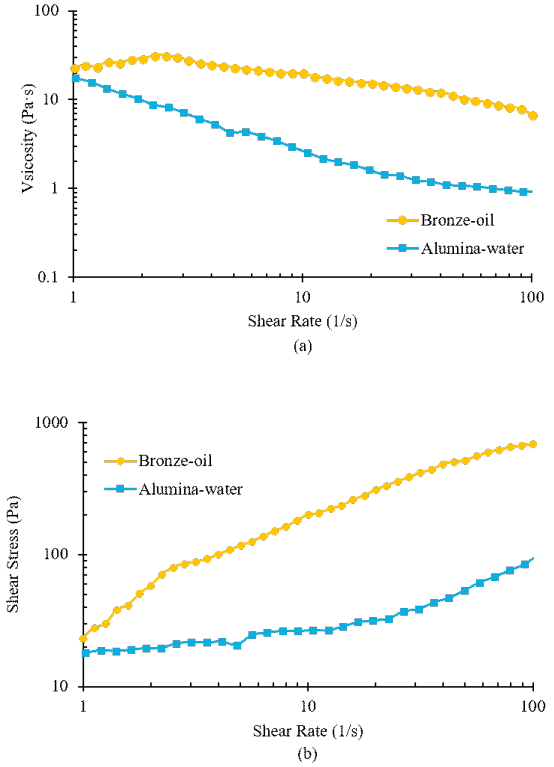

Fig. 8. Rheological properties of a 40 wt.% alumina-water suspension and a 94% bronze-oil suspension on a logarithmic scale: (a) viscosity-shear rate curves; (b) shear stress-shear rate curves.

3.2 The effects of extrusion pressures p and printing nozzle speed v on extruded filament size

The effects of extrusion pressure p and printing nozzle speed v on extruded filament size were studied by extruding a 94wt% bronze-oil suspension in a 40wt% alumina-water suspension at different extrusion pressures p (2 ~ 8 Pa) and printing nozzle speeds v (2 ~ 8 mm/s). A 20 Gauge nozzle (i.e., 0.61 mm inside diameter and 0.91 mm outside diameter) was used. After drying, the powder bed was cut in half to display the cross-sections of the extruded filaments. The resulting filament diameters y were measured. The experiment results are given in Fig. 9.

As can be seen in Fig. 9a, the achieved bronze filament size after drying is proportional to the applied extrusion pressure. In contrast, the achieved bronze filament size is inversely proportional to the square root of the printing nozzle speed, as shown in Fig. 9b. Based on the experimental results, bronze filament size achieved through the 20 Gauge nozzle can be expressed as the following equation:

$$y \approx 250\sqrt{2} * p * v^{-0.5} \quad (1)$$

in which:

- y is the filament size (unit: μm);
- p is the extrusion pressure (unit: *psi*);
- and v is the printing nozzle speed (unit: *mm/s*).

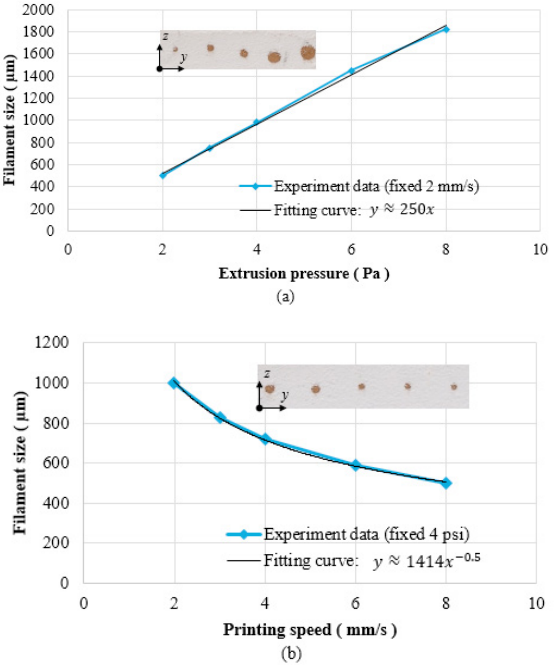

Fig. 9. Effects of (a) extrusion pressure and (b) printing speed on extruded filament size.

3.3 The effects of printing nozzle speed v on filament deformation

Even though a bronze suspension can be self-stabilized within the alumina matrix suspension after extrusion, extruded bronze suspension filaments are still subjected to deformations caused by nozzle movement during the fabrication process and capillary force of liquid during drying. We thereby examined the effects of nozzle moving speed v and liquid phase drying on extruded bronze filaments. The experiment methods and results are shown in Fig. 10.

The effects of nozzle moving speed v on extruded bronze filaments were experimentally studied as follows: six filaments of a 94wt% bronze-oil suspension were first extruded (extrusion pressure p = 4 *psi*) in parallel along the y-axis in the horizontal plane (the x-y plane) within a 40wt% alumina-water suspension, as described in Fig. 10a. Then the nozzle was reinserted into the alumina-water suspension at a height of 1~2 mm above the extruded filaments and moved along the x-axis with different speeds (1~10mm/s). The powder bed was then dried and cut along the x-y plane to show the deformation of filaments of dry bronze particles. The results given in Fig. 10c suggest that a nozzle speed v greater than 4mm/s leads to a macroscopically obvious distortion of a bronze-suspension filament deposited underneath. In the following experiments, a

nozzle speed of 2 *mm/s* was set to minimize its effect on previously-deposited filaments.

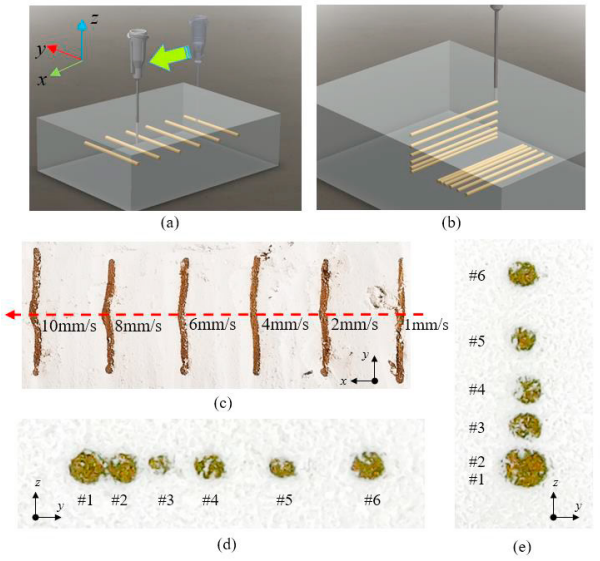

Fig. 10. (a) and (b) Schematic illustrations of experiment setups; (c) effects of nozzle moving on neighbor filaments; (d) and (e) effects of liquid phase drying on relative positions between adjacent filaments.

3.4 The effects of liquid-phase drying on filament deformation

The effects of liquid-phase drying on filament deformation were studied by examining the changes of distances between parallel filaments before and after drying. Filaments were extruded (extrusion pressure $p = 4$ *psi*) in parallel in both x-y and x-z planes with different distances increasing from 0.5 *mm* to 1.5 *mm,* as depicted in Fig. 10b. Final results are shown in Fig. 10d (horizontal direction) and 10e (vertical direction). The values for the final distances are given in Table 2. The average filament diameter was measured as 0.75 *mm*.

Table 2. Distances (mm) between adjacent filaments before and after drying

		#1-2	#2-3	#3-4	#4-5	#5-6
Design		0.50	0.75	1.00	1.25	1.50
After drying	Horizontal	0.75	0.85	1.05	1.75	2.00
	Vertical	0.17	0.86	0.94	1.14	1.50

According to Table 2, the final distances between adjacent filaments along the horizontal direction are greater than the designed distances. This slight increase is due to the influence of stress fields introduced by the nozzle movement during filament extrusion. On the contrary, the final distances between adjacent filaments along the vertical direction are smaller than the designed settings. This can be explained by the anisotropic drying shrinkage of the powder bed along the vertical direction. In addition, the greater decrease in the distance between #1 and #2 filaments along the vertical direction may be explained by the coalescence of the two filaments under surface tension. The increase in the distance between #2 and #3 filaments along the vertical direction should be due to measurement errors considering #2 filament merged with #1 filament.

3.5 Path planning at intersection points

Furthermore, path planning strategies at intersection points of two filaments have been studied. As shown in Fig. 11, a 94wt% bronze-oil suspension with a cross shape was extruded in the horizontal plane in a 40wt% alumina-water suspension along two different paths, i.e., path A and B. In path A, filament 2 was directly extruded across filament 1. In path B, each filament was extruded with a 90-degree turn and met in the intersection. The results after drying in Fig. 11 indicate that path A can avoid disconnection of the two intersecting extrusions.

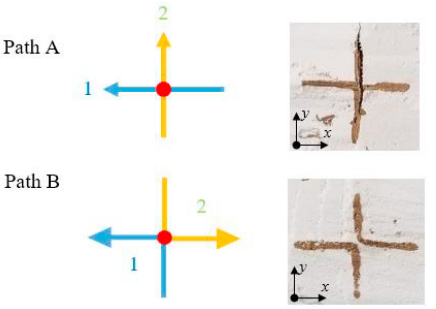

Fig. 11. Path planning strategies for intersecting filaments

4. Case Study

In this section, several testcases were fabricated to verify the capability of the presented II-DMD process. Fig. 12a shows a bronze lattice structure, which can be used as structural frames of micro robots. Fig. 12b shows a stent structure, which can be applied to prop up a pathological changed blood vessel in the human body if shape memory alloy powder is used. These testcases suggest potential applications of our process in fabricating metal/alloy lattice and truss structures.

To further demonstrate the capability of the II-DMD process, two cone springs with different sizes were printed and shown in Fig. 12c. An optical microscope image of the external surface of the springs is shown in Fig. 12d. The rough surface finish is mainly caused by a large bronze particle size (with a diameter of 44 μm) used in the process. Scanning electron microscope (SEM) images of the spring specimens are shown in Fig. 12e and 12f. It can be seen that small pores with diameters around 10 to 40 μm exist in the cross section, which may be caused by inappropriate selection of bronze particle size and drying parameters.

Mechanical properties of fabricated metal structures were determined using a tensile tester (100 series UTM, TestResources

Inc., Shakopee, MN USA). Three bronze filament specimens (with a diameter of 1 *mm* and a length of 40 *mm*) were built. A slow strain rate of 2.54 *mm/min* was applied due to a small diameter of the specimens. The testing results are given in Fig. 12g and Table 3. The results show the bronze material fabricated by our method possesses a maximum yield strength of 126 MPa and a maximum ultimate strength of 188 MPa. In addition, the density of fabricated specimens was measured by the Archimedes method (ASTM C373-88). The result shows an average density of 95.5% of the density of raw Tin Bronze.

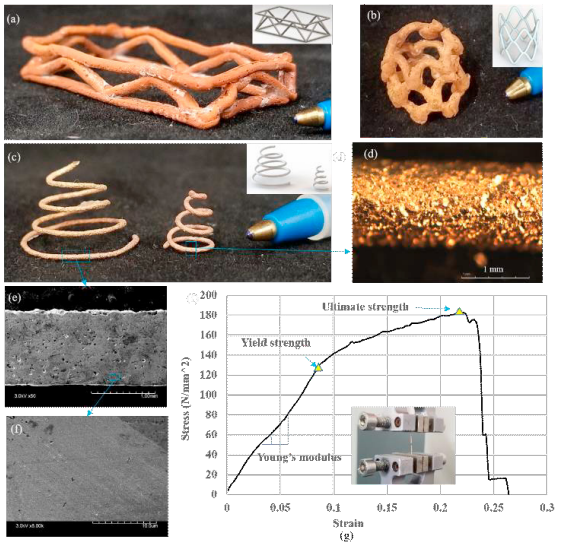

Fig. 12. Test cases: (a) a lattice structure, (b) stent structure, (c) cone springs, (d) optical microscope image of springs, (e) and (f) SEM images of printed samples, (g) tensile test of a fabricated specimen.

Table 3. Mechanical properties of bronze filaments achieved by the II-DMD process

Properties	Printed bronze specimen	C90300 Tin Bronze[19]
Yield strength	110 ± 16 MPa	145 MPa
Ultimate strength	158 ± 30 MPa	310 MPa
Elongation	30 ± 10 %	30%
Density	8200 ± 200 Kg/m^3	8800 Kg/m^3

5. Conclusion and Future Work

In this article, we report a layerless AM process for metal and alloy lattice fabrication, in which an immiscible interface and unique rheological behaviors of highly-loaded metal and ceramic colloidal suspensions are utilized to build complex metal lattice structures. It can potentially fabricate numerous metal alloy materials without generating staircase effect and the need of support structures, and the microstructures of achieved metal alloy parts can potentially be homogeneous and isotropic. Bronze materials are used as a model material to demonstrate the process, with alumina powder as a matrix material. The experimental study suggests that an alumina-water matrix suspension with a solid loading from 35wt% to 40wt% and a bronze-oil suspension with a solid loading of 94% achieves a desired self-stabilization of the material system after extrusion.

However, some limitations of the II-DMD process should be noted: (1) Accuracy. The accuracy of the II-DMD process is influenced by the flow deformation and recovery of the ceramic matrix suspension around the moving nozzle. Material and process parameters can be optimized to minimize the local deformation of the ceramic matrix suspension and thus eliminate distortion of printed metal filaments. (2) Surface finish. Surface finish is mainly determined by the interaction between two colloidal suspensions. In this work, we used a ceramic particle size of 9 µm and a metal particle size of 44 µm. The interaction between such large particles leads to the rough surface finish of the resulting bronze materials. Future work will study how the particle interaction at the immiscible interface will influence surface finish of final parts. (3) Porosity. The achieved parts of this work possess a porosity of 5%, which can be further improved by optimizing the feedstock and sintering process. In addition to these limitations, fundamental physics behind the II-DMD process will be numerically and experimentally studied and more materials will be tested. Applications in fabricating biomedical devices will be further explored.

Acknowledgement

The authors acknowledge Prof. M.L. Raghavan at UI, Mr. Matthew Selman and Mr. Pete Moscatelli at TestResources Inc. for their help with mechanical testing.

References

[1] Gu, D., Meiners, W., Wissenbach, K., and Poprawe, R., 2012, "Laser additive manufacturing of metallic components: materials, processes and mechanisms," International materials reviews, 57(3), pp. 133-164.

[2] Strößner, J., Terock, M., and Glatzel, U., 2015, "Mechanical and Microstructural Investigation of Nickel-Based Superalloy IN718 Manufactured by Selective Laser Melting (SLM)," Advanced Engineering Materials, 17(8), pp. 1099-1105.

[3] Chen, H., Gu, D., Dai, D., Ma, C., and Xia, M., 2017, "Microstructure and composition homogeneity, tensile property, and underlying thermal physical mechanism of selective laser melting tool steel parts," Materials Science and Engineering: A, 682, pp. 279-289.

[4] Bhattacharjee, T., Zehnder, S. M., Rowe, K. G., Jain, S., Nixon, R. M., Sawyer, W. G., and Angelini, T. E., 2015, "Writing in the granular gel medium," Science Advances, 1(8).

[5] Esser-Kahn, A. P., Thakre, P. R., Dong, H., Patrick, J. F., Vlasko-Vlasov, V. K., Sottos, N. R., Moore, J. S., and White,

S. R., 2011, "Three - Dimensional Microvascular Fiber - Reinforced Composites," Advanced Materials, 23(32), pp. 3654-3658.
[6] Grosskopf, A. K., Truby, R. L., Kim, H., Perazzo, A., Lewis, J. A., and Stone, H. A., 2018, "Viscoplastic Matrix Materials for Embedded 3D Printing," ACS Applied Materials & Interfaces.
[7] Hanson Shepherd, J. N., Parker, S. T., Shepherd, R. F., Gillette, M. U., Lewis, J. A., and Nuzzo, R. G., 2011, "3D microperiodic hydrogel scaffolds for robust neuronal cultures," Advanced functional materials, 21(1), pp. 47-54.
[8] Moravej, M., and Mantovani, D., 2011, "Biodegradable metals for cardiovascular stent application: interests and new opportunities," International journal of molecular sciences, 12(7), pp. 4250-4270.
[9] Subramanian, V., Fréchet, J. M., Chang, P. C., Huang, D. C., Lee, J. B., Molesa, S. E., Murphy, A. R., Redinger, D. R., and Volkman, S. K., 2005, "Progress toward development of all-printed RFID tags: materials, processes, and devices," Proceedings of the IEEE, 93(7), pp. 1330-1338.
[10] T., M. J., M., V. D., L., T. R., Yiğit, M., B., K. D., J., W. R., and A., L. J., 2014, "Embedded 3D Printing of Strain Sensors within Highly Stretchable Elastomers," Advanced Materials, 26(36), pp. 6307-6312.
[11] Wehner, M., Truby, R. L., Fitzgerald, D. J., Mosadegh, B., Whitesides, G. M., Lewis, J. A., and Wood, R. J., 2016, "An integrated design and fabrication strategy for entirely soft, autonomous robots," Nature, 536, p. 451.
[12] Willie, W., Adam, D., and A., L. J., 2011, "Omnidirectional Printing of 3D Microvascular Networks," Advanced Materials, 23(24), pp. H178-H183.
[13] Paunov, V. N., Al-Shehri, H., and Horozov, T. S., 2016, "Attachment of composite porous supra-particles to air–water and oil–water interfaces: theory and experiment," Physical Chemistry Chemical Physics, 18(38), pp. 26495-26508.
[14] Sharp, E. L., Al-Shehri, H., Horozov, T. S., Stoyanov, S. D., and Paunov, V. N., 2014, "Adsorption of shape-anisotropic and porous particles at the air–water and the decane–water interface studied by the gel trapping technique," RSC Advances, 4(5), pp. 2205-2213.
[15] Frazier, W. E., 2014, "Metal additive manufacturing: a review," Journal of Materials Engineering and Performance, 23(6), pp. 1917-1928.
[16] Hussein, A., Hao, L., Yan, C., Everson, R., and Young, P., 2013, "Advanced lattice support structures for metal additive manufacturing," Journal of Materials Processing Technology, 213(7), pp. 1019-1026.
[17] Muth, J. T., Vogt, D. M., Truby, R. L., Mengüç, Y., Kolesky, D. B., Wood, R. J., and Lewis, J. A., 2014, "Embedded 3D printing of strain sensors within highly stretchable elastomers," Advanced Materials, 26(36), pp. 6307-6312.
[18] He, L., and Song, X., 2018, "Supportability of a High-Yield-Stress Slurry in a New Stereolithography-Based Ceramic Fabrication Process," JOM, 70(3), pp. 407-412.
[19] MatWeb, 2019, "Tin Bronze UNS C90300, Copper Casting Alloy."